Theor Chem Acc (2012) 131:1262
DOI 10.1007/s00214-012-1262-3

REGULAR ARTICLE

A classical versus quantum mechanics study of the OH + CO → H + CO_2 ($J = 0$) reaction

E. García · F. J. Aoiz · A. Laganà

Received: 5 June 2012 / Accepted: 19 July 2012 / Published online: 11 August 2012

Abstract Quasiclassical trajectory calculations have been performed for the OH + CO reaction at zero total angular momentum and collision energies up to 0.4 eV. Calculations have been carried out on the same potential energy surface which was used for full-dimensional state-to-state quantum dynamical calculation. The resulting quasiclassical total reaction probability as well as the product rotational and vibrational distributions have been analyzed and compared with the outcomes of a pseudo-quantization treatment of the product vibrational energy. Energy-conserving classical trajectories reproduce fairly well all the quantum features but the oscillatory patterns, whereas this does not apply to the energy non-conserving ones. Total reaction probabilities obtained from quasiclassical calculations at several fixed total angular momentum are also compared with centrifugal sudden quantum results. These results have also allowed to investigate the effect of the total angular momentum on the translational energy and angular distributions of the products.

E. García (✉)
Departamento de Química Física, Universidad del País Vasco (UPV/EHU), 01006 Vitoria, Spain
e-mail: e.garcia@ehu.es

F. J. Aoiz
Departamento de Química Física, Facultad de Química, Universidad Complutense, 28040 Madrid, Spain
e-mail: aoiz@quim.ucm.es

A. Laganà
Dipartimento di Chimica, Università di Perugia, 06123 Perugia, Italy
e-mail: lag@dyn.unipg.it

Keywords Molecular reaction dynamics · OH + CO reaction · Quasiclassical trajectories · Product distributions · Chemistry on grid

1 Introduction

The comparison of calculated and experimental data of the kinetics and dynamics of a chemical reaction is the usual way to validate its potential energy surface (PES) and rationalize its dynamical behavior. The OH + CO reaction is an ideal benchmark for this purpose because, due to its importance in modeling combustion and atmospheric chemistry, a great deal of kinetics and dynamical results are available.

Thermal rate coefficients of the title reaction were measured in a wide interval of temperature (80–2,800 K) [1]. Related values display a marked non-Arrhenius behavior with a significant activation energy at high temperatures and a rather flat dependence at low temperatures. Kinetics studies were also performed to investigate the role played by initial vibrational excitation of the OH and CO reactant molecules [2, 3]. The CO vibrational excitation was found to be ineffective in enhancing reactivity. In contrast, when OH is promoted to the first excited vibrational state, the reactivity increases by a factor of seven at room temperature. As for the experiments on the reaction dynamics, Casavecchia and coworkers used a cross molecular beam (CMB) apparatus detecting the CO_2 product by mass spectrometry. By deconvolution of the measured angular and time-of-flight distributions, they extracted the product angular distribution (PAD) in the center-of-mass (CM)—where the scattering angle was defined as that between the OH initial velocity and the CO_2 final velocity—and the product translational energy

distribution (PTD) at 0.37 and 0.61 eV collision energy, E_{tr}, [4–6]. The CO_2 CM–PADs so determined exhibit a bimodal forward–backward structure with a strong forward bias. The two CM–PTDs peak at approximately the same product translational energy ($E'_{tr} = 1.2$ eV) with the low collision energy distribution being narrower than that at high E_{tr}.

Disagreement between theory and experiment could be attributed either to an inaccuracy of the PES or to an approximation built in the dynamics method (or both). Efforts in both directions—improvement on the PES and on the dynamical calculation methodology—have been undertaken in the last decade. Over this period, three full-dimensional ab initio PESs (YMS [7], LTSH [8], and Leiden [9]) were proposed for their use in reactive scattering calculations. Very recently, a new full-dimensional PES, not yet available for distribution, has been published [10, 11]. All these PESs exhibit several stationary points and multiple reaction paths. In particular, they contain two deep wells, associated with the *cis*- and *trans*-HOCO conformers, respectively. The deepest well, associated with the *trans*-HOCO configuration, is separated from products by a barrier higher than that separating the two conformers. Moreover, the path connecting the *trans*-HOCO well to products exhibits another (lower) barrier near a C_{2v} $H-CO_2$ configuration. At this point, it can be mentioned that, as it has been documented for triatomic systems [12–14], the presence of a double well in a PES is a salient feature leading to competition between the associated pathways with interesting dynamical and stereodynamical consequences.

Kinetics and dynamics calculations on the above-mentioned PESs were carried out in the past using mainly quasiclassical trajectory (QCT) calculations [8, 10, 15–18]. Some quantum mechanical (QM) calculations, either of the reduced dimensionality type [19, 20] or limited to zero total angular momentum ($J = 0$) [15, 21–23], have been also performed. In particular, only, very recently, some full-dimensional state-to-state calculations were published [21–23].

Existing calculations are not capable of reproducing all the information derived from experiments. For example, the QCT rate coefficients underestimate and overestimate the measured data at low and high temperatures, respectively [10, 15, 16]. Even, QM calculations do not reproduce either the measured values of the rate coefficient [10, 22]. Theoretical estimates of CM–PTDs and CM–PADs were calculated only using QCT, and they differ significantly from the experimentally derived ones. In particular, QCT CM–PADs calculated on the YMS and LTSH PESs are more symmetric than those derived from the CMB experiment [8, 16], and those calculated on the Leiden PES do not exhibit the forward–backward pattern [17]. All QCT CM–PTDs peak at significantly lower product translational energy; that is, QCT calculations underestimate the fraction of available energy released as translation and overestimate the fraction released as internal energy—even on the most recent PES [11], the QCT calculations predict a considerably smaller release in translation than that deduced from the experiment. The agreement between QCT and experimental CM product distribution results does not improve substantially when pseudo-quantization methods of the product vibrational energy are adopted [18]. Attempts to eliminate possible uncertainties associated with the deconvolution procedure were made by implementing a computational procedure to simulate the outcome of the raw experimental data in the laboratory frame using the theoretical results in the CM frame (the so-called last mile of the molecular reaction dynamics virtual experiment) [24–27]. This has partially modified the emphasis on the agreement (or disagreement) of the calculated CM properties with the corresponding value derived from the experiment—for example, the simulation of the raw laboratory angular and time-of-flight distributions carried out using the QCT results on the Leiden PES do not differ appreciably from those calculated on other PESs despite the corresponding poorer reproduction of the CM–PADs derived from the experiment. In addition, it is worth mentioning that the species detected in the experiment is the heavier product (CO_2), and therefore, the resolution imposed by the kinematics of the experiment (Newton sphere) is much more restricted than that would have resulted from the detection of the light fragment (H).

It still remains open the problem of the reliability of the QCT results when used to judge the quality of a given PES by comparison with the experimental data. A sound assessment would require full-dimensional calculations on the same PES, with all the possible Coriolis couplings and converged on the total angular momentum quantum number J. In addition, the determination of state-to-state integral and differential cross sections would imply the calculation of the full S matrix for all partial waves. Unfortunately, at present, such calculations for the title reaction are too demanding computationally to be feasible. Yet, some years ago, full-dimensional quantum $J = 0$ and reduced dimensionality estimates of the total reaction probability became available and fueled several comparisons of QCT and QM results [15, 20, 28–30]. More recently, however, $J = 0$ full-dimensional state-to-state time-dependent wave packet QM calculations were performed using the LTSH PES, and product energy distributions were computed [21–23]. In particular, besides the evaluation of the reaction probabilities as a function of the collision energy for the ground rovibrational and the first excited vibrational states of both reactants, these calculations provided the average rovibrational energy of CO_2 as a

function of the collision energy, plus the separated product vibrational (PVD) and rotational (PRD) distributions at some collision energies. In addition, QM calculations of ref. [22] provided reaction probabilities from the Centrifugal Sudden (CS) approximation [31, 32]. In this work, thanks to the use of the grid empowered molecular simulator (GEMS) [33] implemented on the European Grid Infrastructure (EGI) [34], it has been possible to run concurrently many large batches of trajectories (hundreds of batches each made of hundreds of thousands trajectories) and perform an extended comparison of QM probabilities with the corresponding QCT, ones in order to assess the suitability of classical methodologies to describe the reactive properties of the $H + CO_2$ reaction.

Two are the main issues addressed in this work. The first one is the investigation of the validity of the QCT method as such and of a recently proposed (and discussed later in more detail) pseudo-quantization method to improve the QCT estimates. To this end, particular attention has been paid to the issue of energy conservation during the trajectory integration. Indeed, a non-negligible number of trajectories integrated on the LTSH PES used in this work lead to a poor conservation of total energy. For this reason, different criteria have been proposed to filter them [8, 16] and the effect of filtering is discussed here. The second main issue addressed in the present work is to ascertain to what extent the $J = 0$ reaction probabilities resemble those calculated for other J values. As an example, it was found in the past that the $H_2 + H_2$ QCT results reproduce the QM reaction probabilities calculated at $J = 0$ [35] fairly well; yet it was also found that the quality of the agreement was strongly dependent on J [36]. In particular, here, we shall focus on the effect of varying total angular momentum on the product distributions as well as on the comparison of the QCT and CS QM results.

The paper is organized as follows. In Sect. 2, details on the calculations are illustrated; in Sect. 3, the QCT and QM total reaction probabilities calculated at $J = 0$ are presented and compared, while in Sect. 4, the comparison is extended to product distributions. In Sect. 5, $J = 0$ dynamical properties are compared with the $J > 0$ and unconstrained ones. Finally, the main conclusions are drawn in Sect. 6.

2 Calculations

As already mentioned, QCT calculations were performed on the same LTSH PES [8], used for the QM calculations of refs. [21, 22]. The LTSH PES is a full-dimensional many-body expansion (MBE) potential [37], whose parameters were determined by fitting ab initio accurate electronic energies. In order to enforce the reproduction of some local structures found in the ab initio data, several Gaussian functions were also added. During the QCT calculations, because of the relatively poor conservation of total energy [8, 16], filtering techniques were adopted by setting a tolerance limit to the deviation of the energy conservation discarding trajectories exceeding such limit. This type of filtering techniques have been already adopted in the past. For example, in ref. [8], only trajectories with an energy conservation better than 5 % of the total energy were retained. The 5 % criterion led to discarding of trajectories with a total energy conservation poorer than 0.086 eV in the case of a collision energy of 0.4 eV and with OH and CO being in their ground states. As a result of this, the calculated value of the cross section slightly differs from that obtained when no filtering was adopted. In ref. [16], a much more restrictive criterion was adopted by enforcing total energy conservation to be better than 0.002 eV. In our work, we adopted the following four different filtering criteria: 5 % (QCT-5 %), 1 % (QCT-1 %), the absolute 0.002 eV (QCT-Cut), and no discarding at all (QCT-All).

QCT calculations have been performed by running a customized version of the program VENUS96 [38] that is a component of the DYNAMICS block of GEMS [33]. This gave us the possibility of exploiting the Grid environment of the European Grid Infrastructure (EGI) [34] for running a massive campaign of QCT calculations (in total, about 2×10^9 trajectories have been integrated). The customized version of VENUS96 incorporates the mentioned LTSH PES routine (as well as those of the YMS and Leiden PESs). To fully reproduce the input of ref. [8], a numerical forward differentiation technique was used to evaluate the derivatives, and a time step of 0.24 fs was adopted to integrate the trajectories. Initial distances were set at 6.3 Å so as to guarantee that the corresponding intermolecular interaction is negligible. The end point of the trajectory integration was set at a distance between the final fragments of 5.3 Å. The impact parameter was set equal to zero. This, together with the null rotational angular momentum of both reactants, ensured a zero total momentum as in the QM calculations. All the remaining parameters (vibrational phases and spatial orientation of molecules) were selected randomly. When QCT calculations at $J > 0$ were performed, the impact parameter was properly set. As an example, a fixed impact parameter of 1.11 AA corresponds to a total angular momentum of 50 at $E_{tr} = 0.4$ eV.

QCT calculations were performed at $J = 0$ for the ground rovibrational state of both OH and CO. Under these conditions, one hundred collision energies spanning the 0.01–0.40 eV interval were considered. At high collision energies, 10^5 trajectories per energy were integrated. This number was raised to 7×10^6 at low collision energies. For the calculation of detailed product distributions, the number

of integrated trajectories was further increased up to 2×10^8. Calculations were also performed for the total angular momentum $J = 30$ and 50. In addition, similar calculations in the same range of E_{tr} values were also carried out for OH and CO excited to their first vibrational state.

The total reaction probability was set equal to the fraction of integrated trajectories leading to H + CO_2. In order to carry out a sound comparison with QM state-resolved results at $J = 0$, detailed product properties were also determined; that is, the rovibrational energy of CO_2, the product rotational state distributions, and the product vibrational state distributions.

Discrete quantum-like vibrational states for the final CO_2 molecule were calculated using the normal mode analysis (NMA) algorithm [39]. The basic idea of the NMA method is to project the final coordinates and momenta of CO_2 onto the respective normal-mode space. It is thus possible to calculate the harmonic vibrational action for each normal mode (the CO_2 molecule involves four modes which correspond to the symmetric and antisymmetric stretching vibrations and to the two degenerate bending modes).

QCT actions are continuous numbers, and therefore, they need to be discretized in order to compare with QM results. In principle, only trajectories starting from reactants and ending with products having nearly integer actions would have to be taken into account. However, in order not to lose the information carried by the trajectories not ending with an exact integer actions, QCT probabilities were obtained by assigning to each individual trajectory a weight, such that the closer is its vibrational action to that corresponding to a quantum (integer) value, the larger is its weight [40, 41]. More in detail, among the different available procedures, the one called one-dimensional Gaussian binning (1GB) [42, 43] has been used in our work. The 1GB method compares the total vibrational energy (rather than the vibrational quantum numbers of each mode) of each trajectory with the corresponding discrete quantum values. In fact, the contribution of a trajectory to a specific vibrational state is given by an one-dimensional Gaussian function centered in the (discrete) harmonic vibrational energy. The 1GB method does not need many trajectories to make the error small. Its theoretical ground for dealing with products bearing several vibrational degrees-of-freedom is given in ref. [44], and its application to the title reaction is described in ref. [18]. Its drawback is the ambiguity associated with the fact that there could be various combinations of vibrational quantum numbers of the different vibrational modes having the same or very close vibrational energy.

QCT trajectories with $J = 0$ were also carried out with both reactants in their ground rovibrational state on the YMS PES [7]. Calculations performed on this PES give the best agreement between QCT and experimental LADs [25]. The YMS PES, alike the LTSH PES, is of the MBE type with various Gaussian functions added to describe some local structures better. The QCT calculations performed on that PES were also affected by a poor conservation of total energy despite the use of analytical derivatives. For this reason, the same filtering criteria used for the LTSH PES were employed. In the QCT calculation on the YMS PES, a time step of 0.24 fs was adopted, and initial and final distances were set at 8.0 Å. The number of trajectories integrated on this PES ranged from 10^5 at high collision energy to 2×10^6 at the lowest ones.

Finally, QCT calculations on both the LTSH and YMS PESs at $J = 0$, 10, 20, 30, 40, 50, and at the ground rovibrational states of both OH and CO were performed at the same collision energies of the CMB experiments ($E_{tr} = 0.37$ and 0.61 eV) in order to estimate both the CM–PTDs and the CM–PADs. More than 2×10^8 trajectories were integrated in each case.

3 Total reaction probability

Figure 1 shows the QCT total reaction probabilities calculated for the title reaction at $J = 0$ with both reactants in their ground rovibrational states. The reaction probabilities are plotted as a function of the collision energy, E_{tr}. For comparison, the figure also includes the most recent QM probabilities (solid line) taken from ref. [21] and various estimates of the total QCT probability based on the already illustrated filtering criteria: QCT-All (results obtained by including all the integrated trajectories), QCT-5 % (results obtained from the application of the 5 % filtering criterion), QCT-1 % (results obtained from the application of the 1 % filtering criterion), QCT-Cut (results obtained from the application of the 0.002 eV filtering criterion). For completeness, QCT-1GB results derived from the QCT-5 % ones by applying the 1GB procedure are also shown. As is apparent from the figure, QCT results adopting the 5 and 1 % filtering, apart from the damping of the QM oscillations, agree well with the QM results of ref. [21], while clearly disagreeing with those of ref. [15] (represented by a long-dashed line). Differences between probabilities obtained from the 'percentage' filtering are small (for example, at $E_{tr} = 0.4$ eV, only 1.3 and 1.6 % of the reactive trajectories are discarded by QCT-5 % and QCT-1 % criteria, respectively, while the number of non-reactive trajectories discarded amounts to 0.1 % for both criteria; at the same time at $E_{tr} = 0.1$ eV the corresponding figures are 6.4 and 14.6 % for the reactive trajectories and 0.4 and 0.7 % for the non-reactive ones). On the contrary, QCT-Cut probabilities underestimate significantly the QM results because the rejection of reactive trajectories

amounts to 67.3 % at $E_{tr} = 0.4$ eV against the 3.8 % of the non-reactive ones, showing the extreme selectivity of this criterion for reactive events. This spells out that a too drastic rejection criterion is a wrong way of dealing with the poor conservation of total energy. Therefore, it is more recommendable to improve the energy conservation by the use of smaller integration steps, at least in the strong interaction region in which the bonds are being broken and formed. The filtering criterion resulting for the use of 1GB method turns out to be also too restrictive. As shown in the plot of Fig. 1, the 1GB method reduces the QCT reaction probability excessively. Another difference between the QM and QCT probabilities lies in the fact that while the QM $J = 0$ reaction probability as a function of E_{tr} seems to exhibit a neat threshold, the QCT one does not. The initial internal energy of reactants in their ground rovibrational states is actually large enough (and apparently of the proper type) to drive the system over the potential energy barrier leading to products. This fact has obvious consequences on the QCT estimates of the low energy cross sections and hence of the low temperature thermal rate coefficients, which are bound to be larger than their QM counterparts. These effects are similar, though less pronounced, to the ones obtained on the better energy-conserving YMS PES.

The QCT calculations of the reaction probability with OH or CO promoted to their first excited vibrational state render similar results to those obtained when both reactants are in their ground vibrational states. The top panel of Fig. 2 shows the comparison of QCT and QM results plotted as a function of the collision energy for the reaction with OH($v = 1$). As can be seen, the QCT-All, QCT-5 %, and QCT-1 % values also reproduce fairly well the QM reaction probability (apart from the oscillations), and it seems to indicate that there is a significant enhancement of the reactivity when energy is allocated into OH vibration. Once more, the QCT-Cut reaction probabilities clearly underestimate the QM results, becoming even larger if the 1GB procedure is applied to discretize the vibrational energy of the products. Also in this case, the energy threshold (if any) is close to zero for QCT probabilities.

The corresponding reaction probabilities for the OH + CO reaction when CO is initially in the $v = 1$ state are shown in the bottom panel of Fig. 2. QCT-All, QCT-5 %, and QCT-1 % curves are within the oscillations of the QM results and do not differ significantly from those obtained when both reagents are in their ground rovibrational state, which is not surprising considering the narrower spacing of the CO vibrational levels.

The agreement between the QCT and QM total reaction probabilities for $J = 30$ and 50 is not as good as that for $J = 0$. In fact, as is apparent in Fig. 3, the QCT-All, QCT-5 %, and QCT-1 % values tend to underestimate the QM results obtained with the CS approximation, especially at high collision energy. This is in line with the fact that CS does not couple the K components (being K the helicity quantum number; i.e., the projection of the total angular momentum **J** onto the body-fixed axis that joins the CM of both molecules). Accordingly, a larger fraction of the

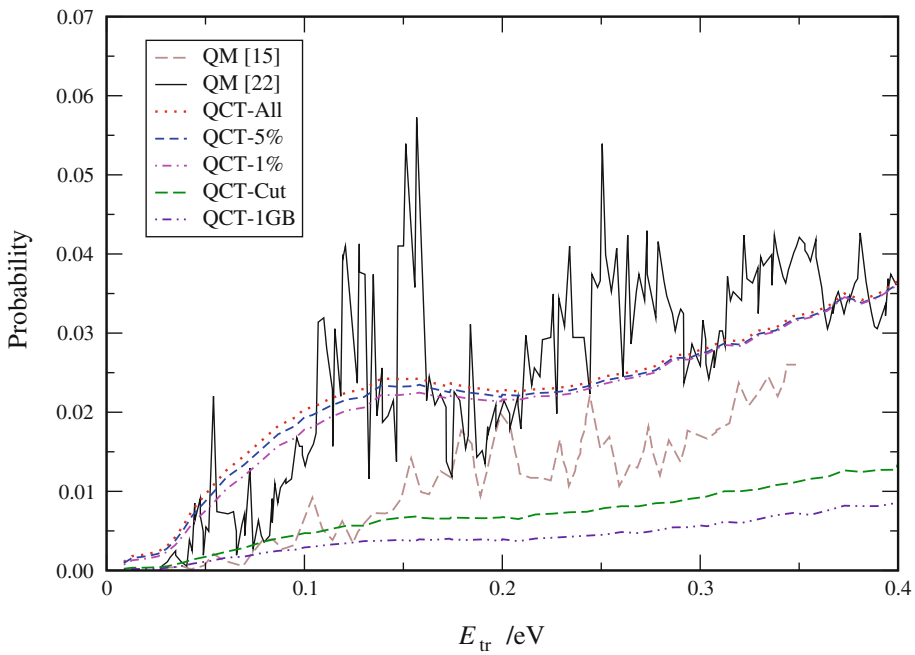

Fig. 1 QCT total reaction probability for OH($v_{OH} = 0$, $j_{OH} = 0$) + CO($v_{CO} = 0$, $j_{CO} = 0$) at $J = 0$ as a function of the initial translational energy. Results obtained when using different filtering criteria for QCTs are reported (see text). QM values of refs. [15, 22] are also shown

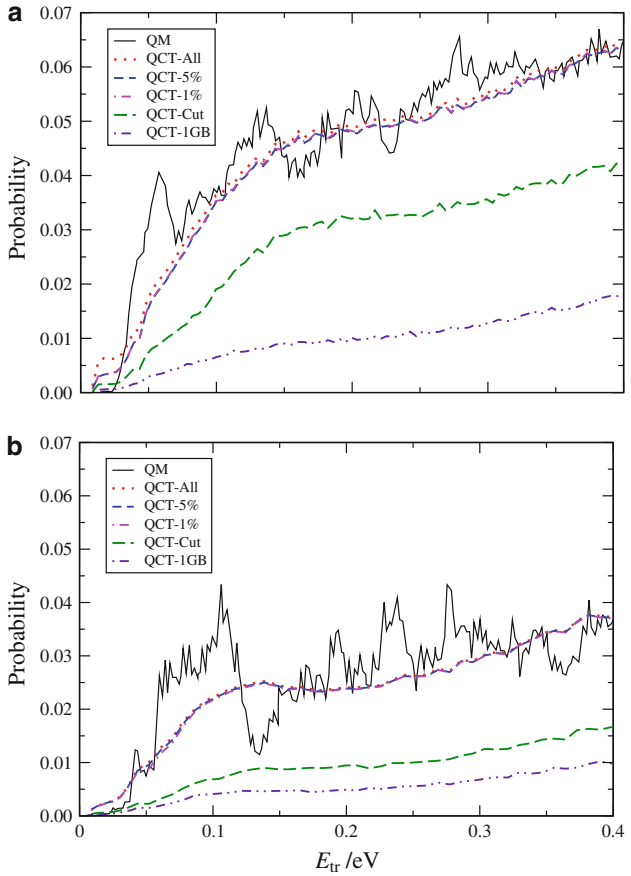

Fig. 2 QCT total reaction probability for OH($v_{OH} = 1$, $j_{OH} = 0$) + CO($v_{CO} = 0$, $j_{CO} = 0$) (*top panel*) OH($v_{OH} = 0$, $j_{OH} = 0$) + CO($v_{CO} = 1$, $j_{CO} = 0$) (*bottom panel*) at $J = 0$ as a function of the initial translational energy. Results obtained when using different filtering criteria for QCTs are reported (see text). QM values of ref. [22] are also shown

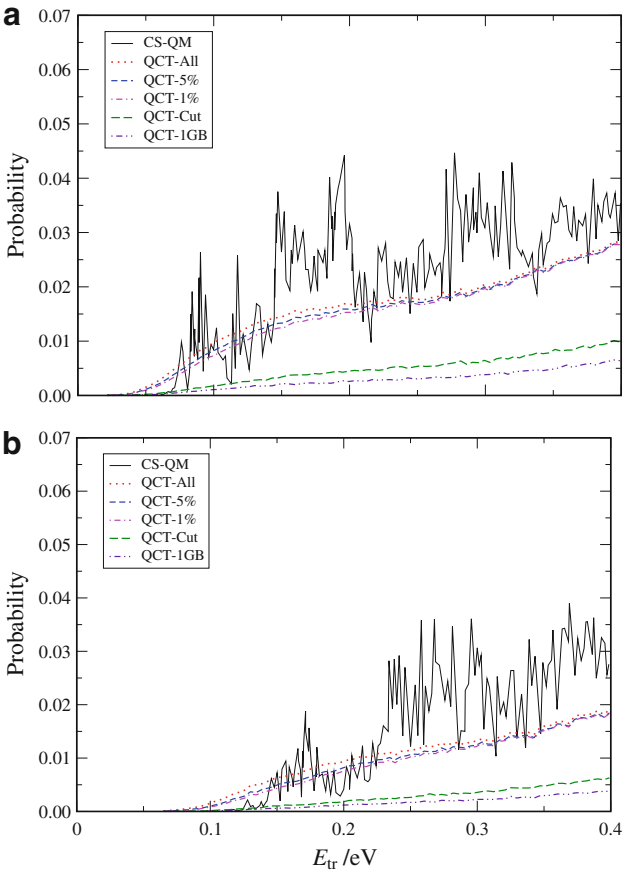

Fig. 3 QCT total reaction probability for OH($v_{OH} = 0$, $j_{OH} = 0$) + CO($v_{CO} = 0$, $j_{CO} = 0$) at $J = 30$ (*top panel*) and $J = 50$ (*bottom panel*) as a function of the initial translational energy. Results obtained when using different filtering criteria for QCTs are reported (see text). CS QM values of ref. [22] are also shown

amplitude of the wavefunction is channeled into $K' = K$, especially for heavy systems. Such deviation is even more evident when QCT-Cut and QCT-1GB results are compared. Another important difference between QCT and CS QM probabilities is again the threshold; the classical value is definitely much smaller.

4 Product energy distribution

To better understand the reactions mechanisms of the title reaction and to investigate whether the QM–QCT agreement so far obtained extends to detailed properties, we have analyzed the average rovibrational energy of CO_2 as well as the rotational (PRD) and vibrational (PVD) product state distributions.

The energy disposed as internal rovibrational energy of CO_2 for OH($v_{OH} = 0$, $j_{OH} = 0$) + CO($v_{CO} = 0$, $j_{CO} = 0$) is plotted in Fig. 4 as a function of the collision energy. The QCT-All results are not included in the plots. In fact, they are off scale because of the anomalous allocation of internal energy in a significant amount of non-energy-conserving trajectories. In contrast, all the other QCT results (the filtered ones) reproduce fairly well the QM results, especially at high collision energy. This implies that while a severe filtering (as that used for the QCT-Cut results) cannot be adopted because, as already shown, it is discriminatory for reactive outcomes, a moderate filtering (or, as commented on above, a shorter integration step size depending on the goodness of the energy conservation) is instead necessary in order to avoid anomalous allocation of the internal energy. Moreover, the comparison shown in Fig. 4 also indicates that the 1GB correction improves the agreement of the QCT with QM results as compared with the standard binning.

Figure 4 also displays the internal rovibrational energy of CO_2 for the ($v_{OH} = 0$, $v_{CO} = 1$) and ($v_{OH} = 1$, $v_{CO} = 0$) cases. When CO is excited to $v = 1$, the agreement between QM and all the QCT results is remarkable

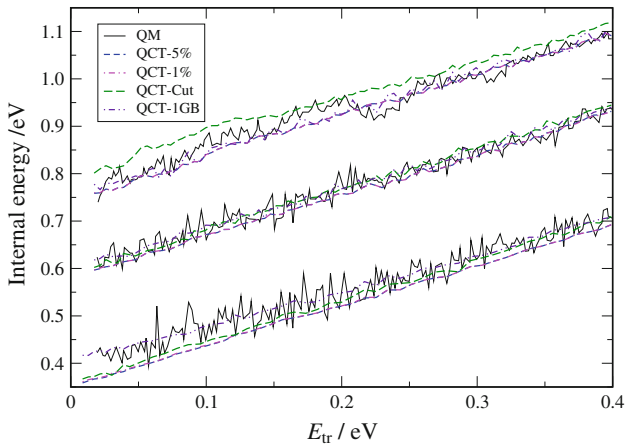

Fig. 4 QCT internal rovibrational energy of CO_2 (including the zero point energy) for $OH(v_{OH} = 0, j_{OH} = 0) + CO(v_{CO} = 0, j_{CO} = 0)$ (*lower lines*), $OH(v_{OH} = 0, j_{OH} = 0) + CO(v_{CO} = 1, j_{CO} = 0)$ (*central lines*), and $OH(v_{OH} = 1, j_{OH} = 0) + CO(v_{CO} = 0, j_{CO} = 0)$ (*upper lines*) at $J = 0$ as a function of the initial translational energy. Results obtained when using different filtering criteria for QCTs are reported (see text). QM values of Ref. [23] are also shown

(except for the QM oscillations), particularly when using the 1GB correction. In the case ($v_{OH} = 1$, $v_{CO} = 0$), despite the fairly good agreement between the QM and QCT reaction probabilities, QCT-Cut results slightly overestimate the QM internal energy in the whole range of collision energies considered here. The good agreement found between QCT and QM results implies that the QCT method describes accurately the effect of the reactants vibrational excitation on the internal energy of the CO_2 product. As a matter of fact, vibrational excitation of reactants results in a significant increase of the internal energy of the product molecule, although its effectiveness is similar to the increase of collision energy (see Fig. 4c in ref. [23] where the internal energy of CO_2 is plotted as a function of the total energy).

To go into detail, we have also analyzed the fraction of the available energy channeled into product translation, vibration, and rotation. As can be seen in Table 1, the fraction of energy disposed as product internal energy in QCT calculations ranges from 30 to 40 %—which increases at the expense of translation—as the collision energy of the reactants increases. However, the fraction of product rotational energy varies about 5 %, a value much higher than the quantum one (0.8 %). Such discrepancy can be attributed to the method used for the calculation of the product rotational energy in ref. [21]. The QM values are, in fact, calculated indirectly from the PRDs by assuming that the CO_2 rotational constant does not change appreciably for the relevant vibrational states. The QCT mean rotational energy of the products can be instead calculated by averaging directly the outcome of the integrated trajectories. The mean rotational energy values computed in this way are 0.0647, 0.0728, 0.0835, and 0.0927 eV for the collision energy of 0.1, 0.2, 0.3, and 0.4 eV, respectively. At the same time, however, the values computed from the PRDs are 0.0088, 0.0105, 0.0123, and 0.0141 eV which compare better with the QM data (namely, 0.0057, 0.0068, 0.0105, and 0.0111 eV) and support our assumption.

When reactants are vibrationally excited, the fraction of total energy disposed as internal energy of CO_2 increases with respect to that obtained when both reactants are in their ground states, with this effect being more evident when OH is vibrationally excited. Moreover, the fraction of internal energy of products increases with the initial translational energy. As a matter of fact, when OH is initially vibrationally excited at the highest energy considered, more than the 50 % of the available energy is channeled as rovibrational energy of CO_2.

In passing, a brief mention to the $J = 0$ QCT product internal energy obtained on the YMS PES for $OH(v_{OH} = 0, j_{OH} = 0) + CO(v_{CO} = 0, j_{CO} = 0)$ is also in order. In this case, the product CO_2 molecule is definitely hotter than that obtained on the LTSH PES for both the QCT and QM treatments. This means that the fraction of total energy disposed as product internal energy on the YMS is lower (as previously obtained also for the all J calculations [24, 25]). Here again, the better energy conservation on the YMS PES is confirmed by the fact that the LTSH QCT-Cut results are practically coincident with the QCT-5 and QCT-1 % ones. Moreover, the fraction of available total energy released as vibration of CO_2 differs depending on the PES used. Actually, despite the fact that the average product

Table 1 QCT fraction of available energy channeled into product translation, vibration and rotation for $OH(v_{OH}, j_{OH} = 0) + CO(v_{CO}, j_{CO} = 0)$ at $J = 0$ calculated on the LTSH PES using the 5 % criterion

E_{tr}/eV	$(v_{OH} = 0, v_{CO} = 0)$			$(v_{OH} = 0, v_{CO} = 1)$			$(v_{OH} = 1, v_{CO} = 0)$		
	f'_{tr}	f'_{v}	f'_{r}	f'_{tr}	f'_{v}	f'_{r}	f'_{tr}	f'_{v}	f'_{r}
0.1	0.691	0.263	0.046	0.600	0.349	0.051	0.547	0.413	0.040
0.2	0.657	0.295	0.048	0.573	0.373	0.054	0.526	0.428	0.046
0.3	0.625	0.324	0.052	0.555	0.389	0.056	0.507	0.443	0.050
0.4	0.596	0.350	0.054	0.528	0.415	0.057	0.491	0.458	0.051

internal energy released on YMS is larger than that estimated on LTSH, the average product rotational energy is lower, making the fraction of the total energy available to the products released as vibration on the LTSH significantly smaller than the corresponding value on the YMS.

QM CO_2 rotational distributions have been also calculated for $J = 0$ at some collision energies and can be compared with QCT ones (see Fig. 5). Only PRDs calculated using the criterion of 5 % and the 1GB procedure are plotted in the figure (QCT-All values are off scale and QCT-1 % results are indistinguishable from the QCT-5 % ones). As can be seen in the figure, the oscillatory behavior of the QM distributions is not reproduced by QCT calculations. In particular, at $E_{tr} = 0.1$ eV, the QM results exhibit a pronounced peak at $j_{CO_2} = 2$ and a smaller one at $j_{CO_2} = 9$ while the QCT curves increase smoothly up to a maximum at $j_{CO_2} = 7$ and then decrease as the rotational angular momentum increases.

The analysis was extended to the PVDs. As an example, Fig. 6 shows the PVDs calculated at the collision energy of 0.1 eV with the 5 % criterion (top panel) and the 1GB procedure (central panel). Please, note that for the sake of simplicity, only the most populated states are considered. This figure also shows the QM PVD distributions in the lower panel. Vibrational states are labeled as (n_1 n_2 n_3), with n_1, n_2, and n_3 being the symmetric stretching, the bending mode, and the antisymmetric stretching mode, respectively. The degeneration of the bending mode

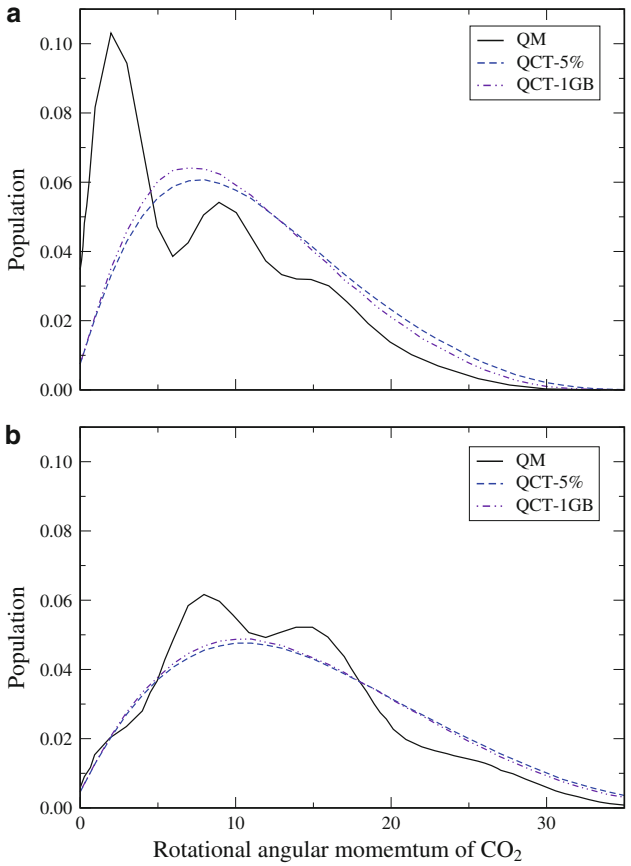

Fig. 5 QCT product rotational distributions of CO_2 for OH($v_{OH} = 0$, $j_{OH} = 0$) + CO($v_{CO} = 0$, $j_{CO} = 0$) at $J = 0$ and $E_{tr} = 0.1$ eV (*top panel*) and 0.4 eV (*bottom panel*). Results obtained when using different filtering criteria for QCTs are reported (see text). QM values from ref. [21] are also shown

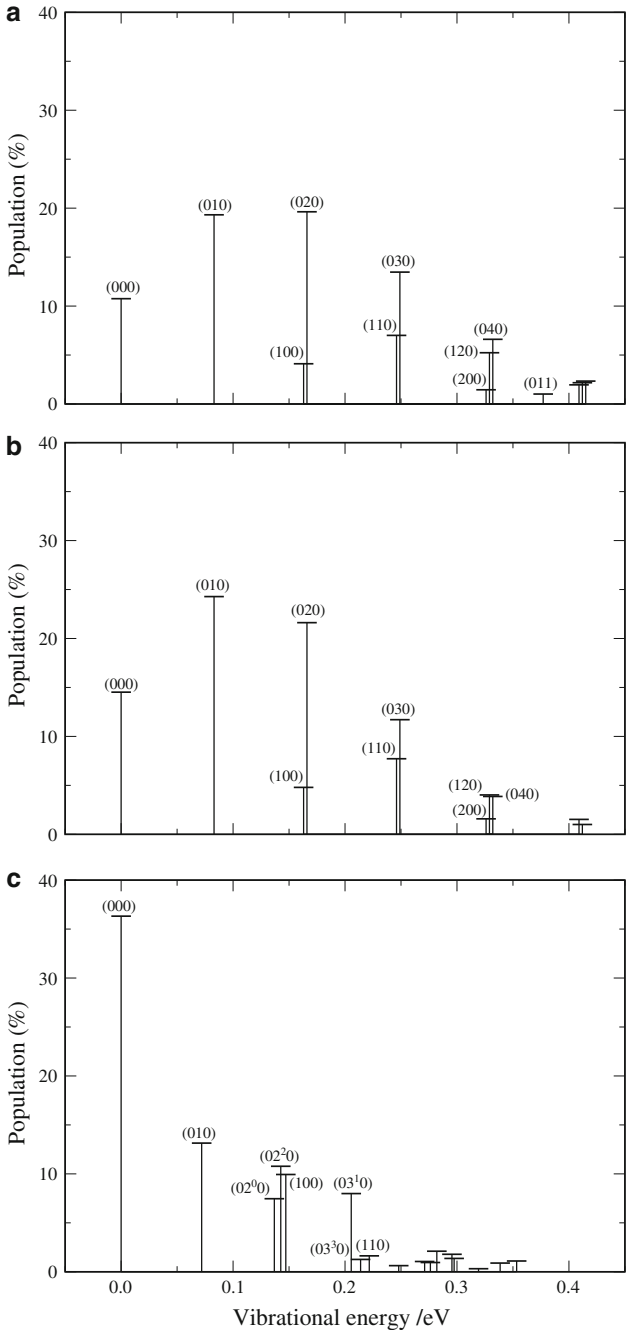

Fig. 6 QCT-5 % (*top panel*), QCT-1GB *middle panel*), and QM [21] (*bottom panel*) product vibrational distributions of CO_2 for OH($v_{OH} = 0$, $j_{OH} = 0$) + CO($v_{CO} = 0$, $j_{CO} = 0$) at $J = 0$ and $E_{tr} = 0.1$ eV

considered by the QM results, which are labeled accordingly, has not been considered in the present QCT calculations.

As is apparent in Fig. 6, non-negligible discrepancies between QCT-5 % and QCT-1GB results can be observed. Former results tend to predict a slightly hotter vibrational distribution than the latter ones. As a matter of fact, QCT-5 % results show a maximum of the product population at (020) contrary to the QCT-1GB maximum, located at (010), and a larger population of the more excited bending states. The disagreement is even more pronounced when comparing QCT and QM results. In particular, the QM PVD has a maximum of population (about 36 %) at the ground vibrational state, against the 10 % one for the QCT-5 % results. As far as the excited vibrational states are concerned, both QCT and QM methods predict an enhancement of the population of the excited bending states (though individual populations differ significantly). Thus, the QCT population of the (010) state is significantly larger than that of the QM one and, although the difference between the populations of the (020) state reduces, the QM progression tends to die faster.

5 Effect of total angular momentum on product distributions

Although the central focus of this work was the rationalization of $J = 0$ dynamical results, because of the lack of exact QM calculations for higher J values, significant efforts have been also devoted to investigate the differences and similarities between QCT results restricted to $J = 0$ and those in which all J values (Jall) are considered. Such comparison can tell us how much $J = 0$ calculations can be representative of the overall dynamics of the title reaction. To this end, the $J = 0$, 10, 20, 30, 40, and 50 CM product distributions computed at the collision energies of the CMB experiment have been compared with the Jall [18] and the experimental results [4–6]. As an example, Fig. 7 shows the related QCT PTDs and PADs calculated on the LTSH PES at the collision energy $E_{tr} = 0.61$ eV and for the ground rovibrational states of both reactants (only results obtained using the 5 % criterion are shown, but the conclusions can be extended to the comparison using different criteria and to the YMS PES as well). The figure shows also the best-fit CM distributions obtained from the CMB measurements (solid line) while the ensemble of functions providing an acceptable fit is represented as a hatched area. QCT PTDs have been obtained using bins of 0.086 eV while PAD bins are 10° wide.

As shown in the upper panel of Fig. 7, the effect of considering only $J = 0$ results leads to a PTD with a shape almost coincident with those of the other fixed Js. All the curves are nearly symmetric with their maximum located at $E'_{tr} = 1.0$ eV with the $J = 0$ curve being slightly wider. Notwithstanding, none of the curves reproduce the experimentally derived PTD that gives a significantly larger fraction of energy disposed in product translation. This feature is usually attributed to an insufficient repulsive nature of the PES in the exit H + CO_2 channel, although, as mentioned in ref. [25], not much emphasis should be put on such disagreement that has been shown to be less important than expected when the comparison is based on the simulation of the laboratory distributions using the theoretical results.

Completely different is the case of the PADs. In fact, the QCT-Jall results exhibit a nearly symmetric forward–backward shape. It is worth noting here that the QCT-5 % PAD (long dashed line) shown in the lower panel of Fig. 7 exhibits a slightly backward bias in contrast with the

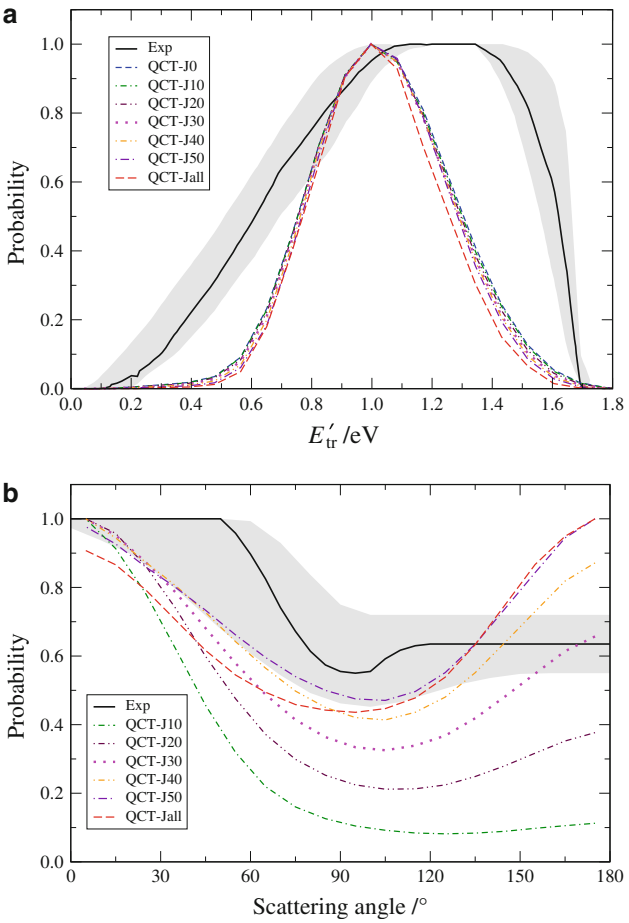

Fig. 7 QCT product translational energy (*top panel*) and angular (*bottom panel*) distributions for OH($v_{OH} = 0$, $j_{OH} = 0$) + CO($v_{CO} = 0$, $j_{CO} = 0$) at $J = 0$, 10, 20, 30, 40, 50 (please, note that in the PAD figure the symbol QCT-J10 refers to the contributions until $J \leq 10$, see text) and $E_{tr} = 0.61$ eV. Experimental distributions of refs. [4–6] are also shown. Distributions are normalized to one in the maximum

slightly forward bias obtained in both ref. [18] (where the QCT-Cut criterion was used) and ref. [8] (where a lower number of reactive trajectories were considered). The QCT-Jall distribution is only qualitatively similar to the experimental one, that is, clearly forward biased.

The shape of the PAD can be better understood by analyzing the building up of the differential cross sections with the successive incorporation of the contributions of more *J*s. Each of these partial summations are plotted in the lower panel of Fig. 7 and labeled as QCT-Jn (where n is the maximum value of *J* considered). As shown in the figure, with increasing value of *J* (from 10 to 50), the shape of the partial PADs varies from clearly forward to nearly symmetric forward–backward. This can be explained by considering that the individual *J* contributions to the PAD are weighted by a $2J + 1$ factor. Therefore, even if lowest *J* contributions are clearly forward biased, the larger *J* ones (starting already from about $J = 30$ in our case) which are backward biased, because of their larger weight, reverse the shape of the PAD.

6 Conclusions

The analysis and/or prediction of experimental quantities is the final goal of the theoretical study of elementary reactions. Ideally, to achieve this objective, the combination of accurate PES and the most possible accurate solution of the full-dimensional Schrödinger equation is required. However, even when accessing to PESs based on high-level ab initio electronic structure calculations is becoming possible, most of the 'exact' theoretical dynamical treatments are still confined to triatomic systems due to the computational complexity of exact dynamical calculations for four or more atoms –the only tetratomic reactive system so far investigated using exact quantum dynamics is the OH + HD one [45, 46], although still neglecting the open shell character of the OH radical. With regard to the $OH + CO \rightarrow H + CO_2$ reaction, a QM exact time-dependent wave packet method was recently applied to calculate the $J = 0$ reaction probabilities, whereas an approximate CS method was applied to determine the $J > 0$ ones. To check to what extent QCT approaches (which are better suited to exploit the distributed features of Grid platforms and perform massive computations) can reliably substitute the exact QM treatment, we have compared $J = 0$ and $J > 0$ results obtained by performing both types of calculations on the LTSH PES.

We found that the $J = 0$ QCT total reaction probability calculated for reactants in the ground and first excited vibrational states reproduces reasonably well the exact QM results in the whole range of collision energy considered here, leaving apart the oscillatory behavior and a somewhat different threshold behavior. We also found that the reproduction of the CS QM total reaction probability is not as good for $J = 30$ and $J = 50$. An important conclusion from this work is that the agreement depends on a large extent on how strictly the conservation of the total energy is enforced, and if non-energy-conserving trajectories were discarded. Somewhat surprisingly, if the discarding is limited to trajectories whose energy deviation is a few percent of the total energy, the state-specific results are similar to those obtained with QM calculations as well as to those with no filter. Yet, it was also found that the enforcing of a more severe (0.002 eV) energy conservation and the adoption of the 1GB discretization method for the product vibrational energy lowers the reactivity excessively (although it hardly affects the non-reactive probabilities). In other words, the adoption of increasingly more drastic energy conservation criteria builds into the dynamical outcome a non-reactive bias. At the same time, however, if no filtering criterion is adopted, no acceptable accuracy can be obtained when evaluating detailed probabilities. A similar result is obtained when the 1GB discretization method is used.

More detailed QM product properties, as the product rotational and vibrational distributions, are also acceptably reproduced by QCT calculations. QCT PRDs exhibit a Boltzmann-like shape and, as expected, are unable to reproduce the QM oscillatory behavior with the presence of several peaks. Analogously, although QCT PVDs predict a preference to populate vibrational states with excited bending as the QM results, they do not reproduce the QM population of the vibrational ground state of CO_2.

Finally, in this paper, we have investigated the effect of total angular momentum on product distributions. The product's translational distributions do not differ appreciably when increasing values of *J* are considered. However, the corresponding computed angular distributions depend significantly on *J*. The QCT individual *J* contributions to the PAD obtained at low values of *J* are, in fact, forward distributions, in contrast to the forward–backward nature of the QCT PAD when all the *J*s are included (this distribution, however, does not reproduce the forward bias suggested by the experiment). As *J* increases, the backward component of the PAD also increases tending to a forward–backward nearly symmetric distribution. Accordingly, we can conclude that caution should be exercised when interpreting detailed spectroscopy or scattering measurements with a limited set of *J*s. Therefore, while on the experimental side, more experiments with higher resolution are needed to further assess the energy dependence of product distributions; on the theoretical side, additional efforts have to be made to calculate exact quantum *S* matrix for higher *J* values.

Acknowledgments The authors acknowledge financial support from Spanish MICINN (CTQ-2008-02578/BQU and Consolider Ingenio 2010 CSD2009-00038), the European EGI-Inspire project (contract 261323), INSTM and Phys4-entry FP7/2007-2013 project (contract 242311). The research leading to the results presented in this paper has been supported by the use of the grid resources and services provided by the European Grid Infrastructure (EGI) and the Italian Grid Infrastructure (IGI).

References

1. Atkinson R, Baulch DL, Cox RA, Crowley JN, Hampson RF, Kerr JA, Rossi MJ, Troe J (1999) J Phys Chem Ref Data 28:191
2. Kohno N, Izumi M, Kohguchi H, Yamakasi K (2011) J Phys Chem A 115:4867
3. Dreier T, Wolfrum J (1981) In: 18th symposium on combustion. The Combustion Institute, Pittsburgh, p 801
4. Alagia M, Balucani N, Casavecchia P, Stranges D, Volpi GG (1993) J Chem Phys 98:8341
5. Alagia M, Balucani N, Casavecchia P, Stranges D, Volpi GG (1995) J Chem Soc Faraday Trans 91:575
6. Casavecchia P, Balucani N, Volpi GG (1995) In: K. Liu, A. Wagner (eds) The chemical dynamics and kinetics of small radicals, World Scientific, Singapore, p 365
7. Yu HG, Muckerman JT, Sears TJ (2001) Chem Phys Lett 349:547
8. Lakin MJ, Troya D, Schatz GC, Harding LB (2003) J Chem Phys 119:5848
9. Valero R, van Hemert MC, Kroes GJ (2004) Chem Phys Lett 393:236
10. Li J, Wang Y, Jiang B, Ma J, Dawes R, Xie D, Bowman JM, Guo H (2012) J Chem Phys 136:041103
11. Li J, Xie C, Ma J, Wang Y, Dawes R, Xie D, Bowman JM, Guo H (2012) J Phys Chem A 116:5057
12. Alvariño JM, Bolloni A, Hernández ML, Laganà A (1998) J Phys Chem 102:10199
13. Martínez T, Hernández ML, Alvariño JM, Aoiz FJ, Saénz-Rábanos V (2003) J Chem Phys 119:7871
14. Gómez-Carrasco S, Hernández, ML, Alvariño JM (2007) Chem Phys Lett 435:188
15. Medvedev DM, Gray SK, Goldfield EM, Lakin MJ, Troya D, Schatz GC (2004) J Chem Phys 120:1231
16. Garcia E, Saracibar A, Zuazo L, Laganà A (2007) Chem Phys 332:162
17. García E, Saracibar A, Laganà A (2011) Theor Chem Acc 128:727
18. García E, Corchado J, Espinosa-García J (2012) Comput Theor Chem 990:47
19. Valero R, McCormack DA, Kroes GJ (2004) J Chem Phys 120:4263
20. Valero R, Kroes GJ (2004) J Phys Chem A 108:8672
21. Liu S, Zhang DH (2011) J Chem Phys 135:234307
22. Liu S, Xu X, Zhang DH (2012) Theor Chem Acc 131:1068
23. Wang C, Liu S, Zhang DH (2012) Chem Phys Lett 537:16
24. Laganà A, Balucani N, Crocchianti S, Casavecchia P, García E, Saracibar A (2001) Lect Notes Comp Sc 6784:453
25. Laganà A, García E, Paladini A, Casavecchia P, Balucani N (2012) Faraday Discuss 157. doi:10.1039/C2FD20046E
26. Martínez T, Hernández ML, Alvariño JM, Laganà A, Aoiz FJ, Menéndez M, Verdasco E (2000) Phys Chem Chem Phys 2:589
27. Bobbenkamp R, Paladini A, Russo A, Loesch HJ , Menéndez M, Verdasco E, Aoiz FJ, Werner HJ (2005) J Chem Phys 122:244304
28. Clary DC, Schatz GC (1993) J Chem Phys 99:4578
29. Goldfield EM, Gray SK, Schatz GC (1995) J Chem Phys 102:8807
30. Valero R, Kroes GJ (2004) Phys Rev A 70:040701
31. Pack RT (1974) J Chem Phys 60:633
32. McGuire P, Kouri DJ (1974) J Chem Phys 60:2488
33. Costantini A, Gervasi O, Manuali C, Faginas-Lago N, Rampino S, Laganà A (2010) J Grid Comput 8:571
34. European Grid Infrastructure, http://www.egi.eu. Accessed 15 May 2012
35. Lu Y, Lee SH, Zhang DH (2006) J Chem Phys 124:011101
36. García E, Saracibar A, Sánchez C, Laganà A (2009) J Phys Chem A 113:14312
37. Murrell JN, Carter S, Farantos SC, Huxley P, Varandas AJC (1984) Molecular potential Energy Functions. Wiley, Chichester
38. Hase WL, Duchovic RJ, Hu X, Komornicki A, Lim KF, Lu D, Peslherbe GH, Swamy KN, Van de Linde SR, Varandas AJC, Wang H, Wolf RJ (1996) QCPE Bull 16:43
39. Corchado JC, Espinosa-García J (2009) Phys Chem Chem Phys 11:10157
40. Bonnet L Rayez J (1997) Chem Phys Lett 277:183
41. Bañares L, Aoiz FJ, Honvault P, Bussery-Honvault B, Launay JM (2003) J Chem Phys 118:565
42. Czakó G, Bowman JM (2009) J Chem Phys 131:244302
43. Czakó G, Kaledin AL, Bowman JM (2010) J Chem Phys 132:164103
44. Bonnet L, Espinosa-García J (2010) J Chem Phys 133179:164108
45. Xiao C, Xu X, Liu S, Wang T, Dong W, Yang T, Sun Z, Dai D, Xu X, Zhang DH, Yang X (2011) Science 333:440
46. Liu S, Xu X, Zhang DH (2012) J Chem Phys 136:144302